Fig. 3.26. Infrared spectra for layers deposited at R = 20.7 and T_d = 200 ºC, after different thermal processing as compared to the as-deposited films. Arrows mark the –OH bonds in the as-deposited samples (a), which are only removed at the 936cm^{-1} band after annealing (b) and partially recovered after aging (c). Under a RTA process, Si-OH bonds no longer appear on the IR spectra.

The change in stress performance regarding annealing processes could be related with variation of film composition. After the first thermal cycle the -OH bands are not observed in the high R samples (Fig. 3.26, spectra b), which can be understood as a decrease of its concentration due to water effusion. As a consequence the film shrinks, becoming the stress less compressive or even tensile, exactly in the same way as the previously described hydrogen effusion at low R's. However, since its impact on the stress value is not so high, it must be compensated by another opposite mechanism. Before analyzing which is this mechanism, it could be useful knowing if the –OH bonds are recovered after the annealing, since if not, it would be a simple way of effusing impurities from the layer without causing much effect over it.

After a complete thermal cycle, samples were exposed to a controlled atmosphere with 85% relative humidity for 65 days. The spectra c of Fig. 3.26 was obtained after this period. Notice that the above-mentioned bands (936cm^{-1}, and 3300-3600cm^{-1}) are partially restored. The behavior of stress with temperature was studied again after the aging process in the controlled atmosphere. The corresponding stress development is presented in Fig. 3.27, showing a partial recovering of the initial stress hysteresis.
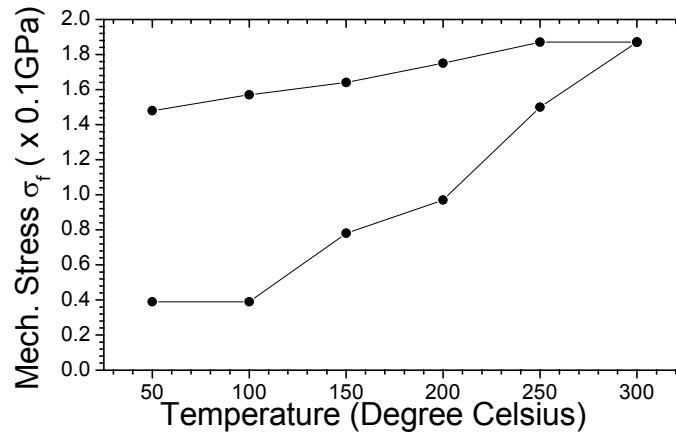
Fig. 3.27. Stress hysteresis for the sample subject to controlled atmosphere.

Fig. 3.28 depicts stress changes in aging time (measured at room temperature). As can be observed, the stress decreases (the structure film-substrate becomes less concave or more convex) but remains positive and reaches a saturation value of approximately 0.02GPa after 35-40 days. All these facts may be associated to a partial re-incorporation of moisture into the film, with a consequent expansion of the film during the exposition to the controlled atmosphere. Thence, after a soft annealing (300ºC) the layer is still able to interact with the atmosphere, recovering, at least partially, its initial properties.
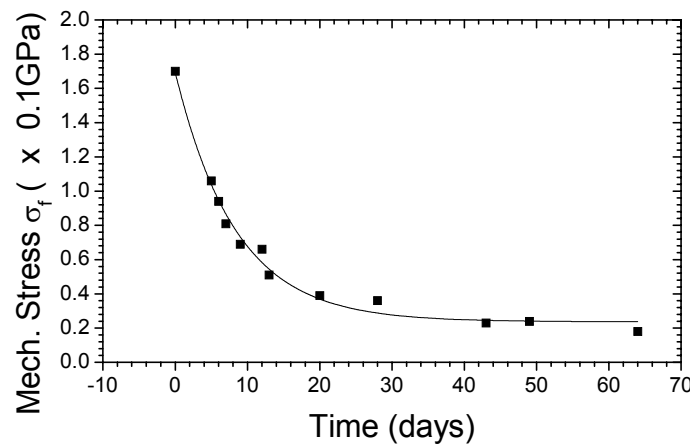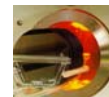

Fig. 3.28. Evolution of stress with aging time in controlled atmosphere.

The observed process of effusion and incorporation of moisture can be satisfactorily explained on the basis of the model proposed in [22] and successfully used in [23]. According to this model three main local environments are proposed for silanol (Si-OH) group in PECVD silicon oxides: near neighbor, partially shielded and completely isolated (by silicon oxide matrix) Si-OH groups. These environments lead to a broad absorption band in the range 3300-3600cm^{-1}. The first one is responsible for the lower wavenumber side of the band as well as the little band at about 936cm^{-1}. It is produced by incorporation of moisture during post deposition exposure of the films at the free atmosphere and results from the attack of strained Si-O-Si groups (commonly encountered in PECVD silicon oxide) by the water molecule. On the contrary, isolated silanol groups contribute to the higher wavenumber side of the broad band and are formed during deposition and/or cooling down of the sample in the deposition chamber. It should be mentioned that only near-neighbor Si-OH groups have an irreversible character during effusion and reincorporation of moisture and, therefore, only a partial recovering of absorption bands and stress value takes place, in accordance to the experimental results. To verify the presence of different local environments for Si-OH groups, new identical layers with R=20.7 were obtained. Special care was taken to measure the infrared spectrum just after the samples were removed from the reactor. Then, they were placed on a controlled atmosphere for a week and the infrared spectra were measured again. Fig. 3.29 depicts the IR results. Notice the presence of the broad band in the approximated interval 3300-3600cm^{-1} as a result of the deposition process and the evolution of the lower wavenumber side of this band as well as the emergence of a little band at about 920cm^{-1} due to absorption of moisture. During aging, a shift of the stretching peak of Si-O bond from 1056cm^{-1} to 1070cm^{-1} was observed in correspondence with the fact that water vapor reacts preferentially with the more reactive group with lower Si-O-Si angles [22] (the typical value of this angle for a relaxed material is about 144º), which correspond to the lower wavenumber side of the peak.

Summing up, for high R values, two different processes are produced during the RTA annealing process: -OH impurity effusion that causes layer to shrink, and

structure reordering, trying to assemble the more energetically favorable SiO_2 tetrahedral, which expands the layer. Due to this competence, the stress variation is not so pronounced at high R as compared to low R. The reason why the reordering does not happen at low R can be due to the fact that they are Si rich layers in which the basic silicon oxide tetrahedral structure is so distorted that it cannot be recovered with a RTA process.
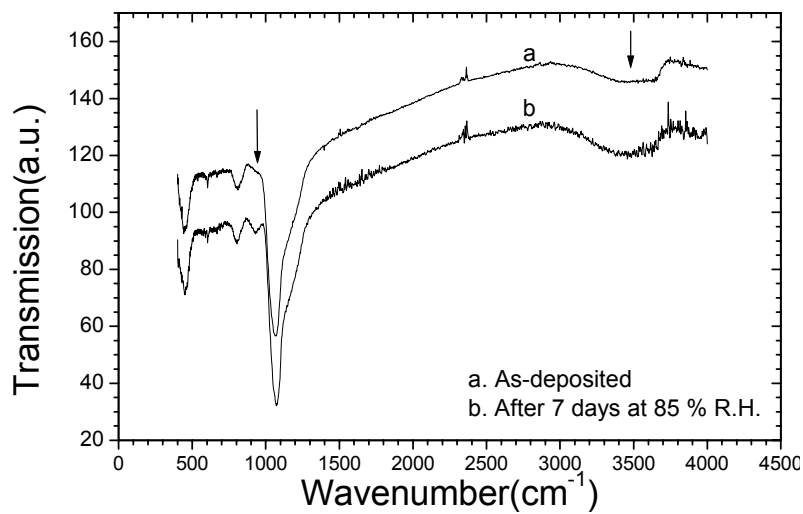

Fig. 3.29. Infrared spectra for samples grown at R = 20.7 and T_d 200 ºC as-deposited (a) and after aging process (b).
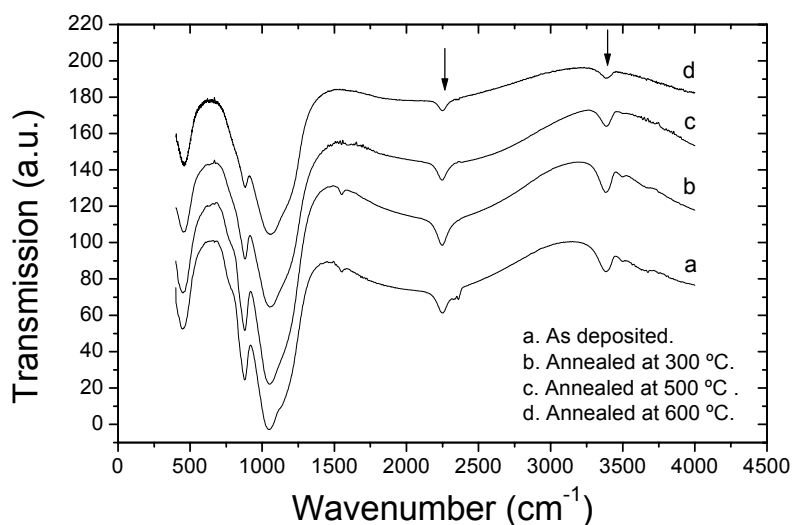

Fig. 3.30. Infrared spectra for as-deposited samples at R = 5.5 and after different annealing processes.

For as-deposited samples at R=5.5 (Fig. 3.30), an important peak at about 3372 cm^{-1} may be ascribed to N-H bonds **[24].** It can also be observed a high concentration of Si-H bonds. No Si-OH bond bands are observed, presumably due to the water blocking mechanism of Si-H bonds proposed by Machida et **al [25]**. Peaks at about 874 cm^{-1} and 2240 cm^{-1} correspond to Si-H bending and stretching vibration bonds, respectively **[24]**. Comparing the position of these peaks with the published data and taking into account that a single peak in the vicinity of 2240 cm^{-1} is observed, it can be concluded that only one tetrahedral unit tip is present, corresponding to the local environment H-Si-O$_3$ **[24]**. Then, silicon is back-bonded to three oxygen atoms and the corresponding Si-H bond band strength is the higher possible. Thus, the hydrogen effusion would require a high temperature. To verify that, a sample deposited with the mentioned parameters was submitted to different successive thermal treatments and the corresponding infrared spectra are shown in Fig. 3.30. After 1 hour annealing at 500°C no appreciable decrease of the Si-H (as well as N-H) bond band is observed. This fact explains the little or almost negligible stress hysteresis observed during thermal cycles up to 300 ºC. According to Fig. 3.30, an annealing at 600 ºC was necessary to detect a significant reduction of the Si-H and N-H bands; they completely disappeared after a RTA process at 900 ºC **[26]**. Therefore, the curvature change, from convex to concave, being found after the RTA process may be considered as a natural result of the film shrinkage due to hydrogen effusion as well as a material reordering taking place during that process. Tensile stress leads usually to a crack of the thicker layers.

The preceding analysis was achieved for samples deposited at 200 ºC. Even though all the effect considered are more pronounced on that case, it should also be considered for every deposition temperatures. Fig. 3.31 depicts the effects of the deposition temperature on the stress hysteresis during the first thermal cycle for samples deposited at R=5.5 and R=20.7. Notice that the hysteresis exists in all cases although it is far larger for the sample with high R, especially if the deposition temperature is low.
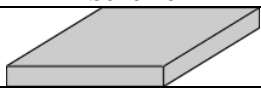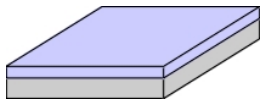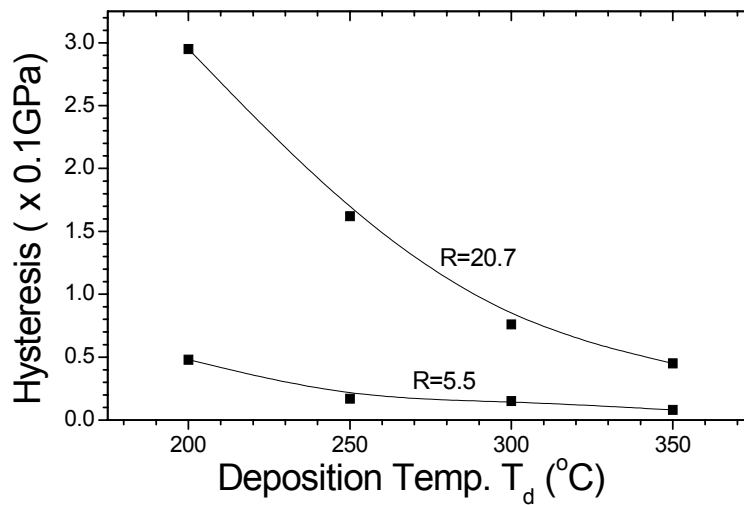
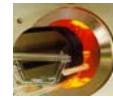**Fig. 3.31**. Stress hysteresis as a function of deposition temperature.

Finally, it has to be pointed out that after RTA, a very stable material is obtained. No detectable change was observed neither on the stress values nor on the FTIR spectra after 8 months exposition under controlled atmosphere. Then, it could be said that the layer has been frozen and that it does not interact with the atmosphere, even if it was deposited at high R. Hence, with an accurate control of the deposition parameters and after analyzing the effect that RTA causes on the films, it has been possible to achieve a 1.0µm silicon oxide impurity-free nearly stoichiometric layer whose properties are non-variant in time.

From the previously obtained results, the process designed that allows obtaining ARROW-A and ARROW-B waveguides are presented in table 3.11.

Scheme	Step properties	
	Silicon substrate: One-side polished, N-type, 4' diameter, 500 µm thick	
	A	**2nd cladding:** 2 µm thermal silicon dioxide **Precursors:** Water vapor **Temperature:** 1100 ºC **Pressure:** 1013 HPa **Growth time:** 9h40' **Refractive index:** 1.46

	B	**2ⁿᵈ cladding:** 2 μm PECVD silicon oxide **Precursors:** N_2O and SiH_4 (R=[N_2O]/[SiH_4]=5) **Temperature:** 300 ºC **Pressure:** 26.6 Pa **Power:** 30 Watt **Growth speed:** 340 Å/min **Refractive index:** 1.56
	A	**1ˢᵗ cladding:** 0.38 μm LPCVD silicon nitride **Precursors:** SiH_2Cl_2 and NH_3 **Temperature:** 800 ºC **Pressure:** 20.0 Pa **Power:** 30 Watt **Growth speed:** 41 Å/min **Refractive index:** 2.00
	B	**1ˢᵗ cladding:** 0.5 μm PECVD silicon oxide. **Precursors:** N_2O and SiH_4 (R=[N_2O]/[SiH_4]=50) **Temperature:** 300 ºC **Pressure:** 26.6 Pa **Power:** 30 Watt **Growth speed:** 210 Å/min **Refractive index:** 1.46
	A	**Core:** 4 μm PECVD silicon oxide **Precursors:** N_2O and SiH_4 (R=[N_2O]/[SiH_4]=8.2) **Temperature:** 300 ºC **Pressure:** 26.6 Pa **Power:** 30 Watt **Growth speed:** 380 Å/min **Refractive index:** 1.48
	B	**Core:** 4 μm PECVD silicon oxide. **Precursors:** N_2O and SiH_4 (R=[N_2O]/[SiH_4]=5) **Temperature:** 300 ºC **Pressure:** 26.6 Pa **Power:** 30 Watt **Growth speed:** 340 Å/min **Refractive index:** 1.56
		Rib definition: 2.5 μm RIE etching with **Precursors:** CHF_3 (50sccm) **Temperature:** Room temperature **Power:** 500 Watt **Pressure:** 5.0 Pa **Etching speed:** 1000 Å/min
		Passivation: 2μm PECVD silicon oxide. **Precursors:** N_2O and SiH_4 (R=[N_2O]/[SiH_4]=50) **Temperature:** 300 ºC **Pressure:** 26.6 Pa **Power:** 30 Watt **Growth speed:** 210 Å/min **Refractive index:** 1.46

Table 3.11: ARROW-A and ARROW-B fabrication steps.

3.6 Cutting & Polishing

When all the processes in clean room have finished, that is, when the devices have been obtained, two remaining steps need to be done: the cutting of the wafer so as to be able to work independently with each chip, and the polishing, that is related to the roughness elimination at the optical devices cross section.

Fig 3.33 Diamond saw cutting technique and equipment used. It causes roughness at the optical device cross section that needs polishing.

Cutting can be done by cleaving from a crystalline plane or using a diamond blade. Cleaving provides completely flat (mirror quality) surfaces since the cut is done by one plane of the substrate crystallographic plane, unfortunately, this cutting method is slow and, if it is manually done, it requires careful handling. If a mechanical diamond blade is used, as shown in fig 3.32, the chip separation can be done automatically, more precise and faster. Concretely, we have used a LOADPOINT 3AV-14. Problems sawing arises from the fact that it is a mechanical cut that causes huge roughness (>50μm). Obviously, an optical device with such an enormous roughness would have unaffordable insertion losses if light was injected to the integrated optical device by end fire coupling. This is the main reason why after the cutting step, integrated optics devices needs to be polished.

Polishing is the final step in the integrated optical device fabrication. As it was previously mentioned, due to the light injection configuration, it is essential that cross section surfaces have as minimum roughness as possible, since the contrary would cause higher insertion losses. For that reason, polishing needs precision. As shown in

fig 3.34, it basically consists on the positioning of the device face that wants to be polished over the surface of an abrasive material that has circular movement. There exist several factors that affect the polishing quality, as can be the chip dimensions, the size of the abrasive particles, the pressure that causes the chip over the abrasive and the angular speed. In our case, it has been used the LECO CORPORATION UP-150 polishing system doing a two-step process. Firstly, a SiC abrasive with grain size of 0.9µm was used for fast polishing of the surface. Once the roughness dimensions was around this value, an alumina abrasive with grain size of 0.3µm was used in order to achieve specular properties of the integrated optical cross section and cause roughness to be lower than the working wavelength.

Fig 3.34 Polishing technique and equipment used so as to eliminate roughness from the optical waveguide cross section.

After cutting and polishing, the cross-section appearance of an ARROW-A is as shown in fig. 3.35, in which instead of the 2µm PECVD silicon oxide layer, a LPCVD 0.12µm-thick silicon nitride has been deposited in order to clearly observe the core profile.
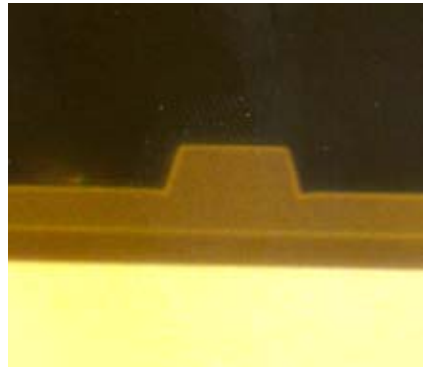
Fig 3.35. ARROW-A structure obtained using the technological processes described.

In this chapter, it has been analyzed all the processes related to the technological aspects of integrated optical devices. It has to be noted, however, that these processes are not exclusive from integrated optics, but the contrary, they come from microelectronics technology and have been adapted so as to fulfill the new requirements. Although indirectly, the order of this chapter was slightly focused on the ARROW-based device fabrication (excepting the evaporative methods at the beginning). Obviously, these processes are not restricted to this waveguide configuration and ARROW configuration could be obtained by several other methods.

Bibliography

[1] T.Suhara, Y.Handa. *Monolithic Integrated Micrograting and Photodiodes for Wavelength Demultiplexing*. Appl.Phys.Lett. 40[20], 120-125. 1982.

[2] W.Stuitus, W.Streifer. *Silicon Nitride Films on Silicon for Optical Waveguides*. Appl.Optics. 16, 3218-3223. 1977.

[3] N.Takato, M.Yasu. *Low-loss High Silica Single Mode Channel Waveguides*. Electr.Lett. 22, 321-323. 1986.

[4] J.Kubica. *Numerical Analysis of InP/InGaAsP ARROW Waveguides Using Transfer Matrix Approach*. J.Light.Tech. 16[6], 767-771. 1992.

[5] Z.M.Mao, W.P.Huang. *An ARROW Optical Wavelength Filter: Design and Analysis*. J.Light.Tech. 11[7], 1183-1188. 1993.

[6] R.A.Soref, K.J.Ritter. *Silicon Antiresonant Reflecting Optical Waveguides*. Opt.Lett. 15[14], 792-794. 1990.
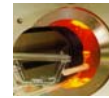
[7] T.Baba, Y.Kokubun. *Dispersion and Radiation Loss Characteristics of Antiresonant Reflecting Optical Waveguides-Numerical Results and Analytical Expressions.* IEEE J.Quant.Elect. 28[7], 1689-1700. 1992.

[8] M.Madou. *Fundamentals of Microfabrication.* CRC Press. 1997.

[9] S.M.Sze. *VLSI Technology.* McGraw-Hill. 1983.

[10] K.K.Schuegraf. *Handbook of Thin-Film Deposition Processes and Techniques. Principles, Methods, Equipment and Applications.* Noyes Publications. 1988.

[11] H.O.Pierson. *Handbook of Chemical Vapor Deposition. Principles, Technology and Applications.* Noyes Publications. 1992.

[12] G.K.Mayer, L.H.Offereins, H.Sandmaier, K.Kuhl. *Fabrication of Non-Underetched Convex Corners is Anisotropic Etching of (100)-Silicon in Aqueous KOH with Respect to Novel Micromechanic Elements.* J.Electrochem.Soc. 137, 3947-3951. 1990.

[13] H.Sandmaier, L.H.Offereins, K.Kuhl, W.Lang. *Corner Compensation Techniques in Anisotrpic Etching of (100)-Silicon Using Aqueous KOH.* Transducers '91 6th International Conference on Solid-State Sensors and Actuators, 456-459. 1991.

[14] C.Burrer. *Design, Fabrication and Characterization of Resonant Silicon Accelerometers*, Thesis. 1995. Universitat Autònoma de Barcelona.

[15] J.A.Plaza. *μAcelerómetros de Silicio*, Thesis. 1997. Universitat Autònoma de Barcelona.

[16] K.Petersen. *Silicon as a Mechanical Material.* Proced.IEEE 70[5], 420-457. 1982.

[17] H.J.Schiliwinski, U.Schnakenberg, W.Kindbracke, H.Neff, P.Lange. *Thermal Annealing Effect on the Mechanical Properties of Plasma-Enhanced Chemical Vapor Deposited Silicon Oxide Films.* J.Electrochem.Soc. 139, 1730-1735. 1992.

[18] M.I.Alonso, M.Garriga, C.Domínguez, A.Llobera. *Characterisation of Complex Multilayer Structures Using Spectroscopic Ellipsometry.* A.Llobera, editor. J.Phys. IV 9[PR8], 1195-1202. 1999.

[19] M.Ohring. *Mechanical Properties of Thin Films. The Materials Science of Thin Films.* Academic Press, Inc. 1991: 403-450.

[20] W.A.Brantley. *Calculated Elastic Constants for Stress Problems Associated with Semiconductors Devices.* J.Appl.Phys. 44[1], 534-535. 1973.

[21] C.Domínguez, J.A.Rodríguez, F.J.Muñoz, N.Zine. *Plasma Enchanced CVD Silicon Oxide Films for Integrated Optics Applications.* Vacuum 52, 395-400. 1999.

[22] J.A.Theil, D.V.Tsu, M.W.Watkins, S.S.Kim, G.Lukovsky. *Local Bonding Environments of Si-OH Groups in SiO_2 Deposited by Remote Plasma-Enhanced Chemical Vapor Deposition and Incorporated by Postdeposition Exposure to Water Vapor.* J.Vac.Sci.Tech A8, 1374-1381. 1990.

[23] M.S.Haque, H.A.Naseem, W.D.Brown. *Correlation of Stress Behavior with Hydrogen-Related Impurities in Plasma-Enhanced Chemical Vapor Deposition Silicon Dioxide Films.* J.Appl.Phys. 82, 2922-2932. 1997.

[24] A.Sasella, A.Borghesi, R.Tonini, B.Pivac, M.Bacchetta, L.Zanoty. *Infrared Study of Si-rich Silicon*

Oxide Films Deposited by Plasma-Enhanced Chemical Vapor Deposition. J.Vac.Sci.Tech. A15, 377-385. 1997.

[25] K.Machida, N.Shimoyama, J.Takahashi, Y.Takahashi, N.Yabumoto, E.Arai. *Improvement of Water-Related Hot-carrier Reliability by Using ECR Plasma-SiO$_2$*. IEEE Trans.Elect.Dev. 41, 709-713. 1994.

[26] C.Domínguez, J.A.Rodríguez, F.J.Muñoz, N.Zine. *The Effect of Rapid Thermal Annealing on Properties of Plasma-Enhanced CVD Silicon Oxide Films*. Thin Solid Films 346, 202-206. 1999.